

# Beyond $\pi$ – $\pi$ Stacking: Understanding Inversion Symmetry Breaking in Crystalline Racemates

Yiran Wang, Matthew L. Nisbet, Kendall R. Kamp, Emily Hiralal, Romain Gautier, P. Shiv Halasyamani, and Kenneth R. Poeppelmeier\*



Cite This: *J. Am. Chem. Soc.* 2023, 145, 16879–16888



Read Online

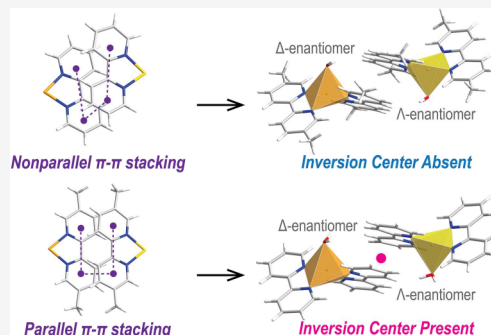
ACCESS |

Metrics & More

Article Recommendations

Supporting Information

**ABSTRACT:** The design of noncentrosymmetric (NCS) solid state materials, specifically how to break inversion symmetry between enantiomers, has intrigued chemists, physicists, and materials scientists for many years. Because the chemical complexity of molecular racemic building units is so varied, targeting these materials is poorly understood. Previously, three isostructural racemic compounds with a formula of  $[\text{Cu}(\text{H}_2\text{O})(\text{bpy})_2]_2[\text{MF}_6]_2 \cdot 2\text{H}_2\text{O}$  ( $\text{bpy} = 2,2'$ -bipyridine;  $\text{M} = \text{Ti}, \text{Zr}, \text{Hf}$ ) were shown to crystallize in the NCS space group  $Pna2_1$ , of polar, achiral crystal class  $mm2$ . In this work, we synthesized five new racemic compounds with the formula  $[\text{Cu}(\text{H}_2\text{O})(\text{dmbpy})_2]_2[\text{MF}_6]_2 \cdot x\text{H}_2\text{O}$  ( $\text{dmbpy} = 4,4'/5,5'$ -dimethyl-2,2'-bipyridine;  $\text{M} = \text{Ti}, \text{Zr}, \text{Hf}$ ). Single crystal X-ray diffraction reveals that the five newly synthesized compounds feature equimolar combinations of  $\Delta$ - and  $\Lambda$ - $\text{Cu}(\text{dmbpy})_2(\text{H}_2\text{O})^{2+}$  complexes that are assembled into packing motifs similar to those found in the reported NCS structure but all crystallize in centrosymmetric (CS) space groups. Seven structural descriptors were created to analyze the intermolecular interactions on the assembly of Cu racemates in the CS and NCS structures. The structural analysis reveals that in the CS structures, the inversion center results from parallel heterochiral  $\pi$ – $\pi$  stacking interactions between adjacent Cu racemates regardless of cation geometries, hydrogen bonding networks, or interlayer architectures, whereas in the NCS structure, nonparallel heterochiral  $\pi$ – $\pi$  interactions between the adjacent Cu racemates preclude an inversion center. The parallel heterochiral  $\pi$ – $\pi$  interactions in the CS structures can be rationalized by the restrained geometries of the methyl-substituted ligands. This work demonstrates that the introduction of nonparallel stacking can suppress the formation of an inversion center for an NCS racemate. A conceptual framework and practical approach linking the absence of inversion symmetry in racemates is presented for all NCS crystal classes.



## INTRODUCTION

The rational design of materials calls for a deep understanding of how atoms, units, or motifs in a crystal structure pack together. Noncentrosymmetric (NCS) solids, in which an inversion center is absent in the structure, are known to display a wide range of functional properties such as nonlinear optical activity, piezoelectricity, ferroelectricity, and pyroelectricity.<sup>1–3</sup> Functional building units (FBUs), such as polar early transition-metal (ETM) octahedra,<sup>4–6</sup> borate clusters,<sup>7–12</sup> polyanions,<sup>13–15</sup> and  $\pi$ -conjugated units,<sup>16,17</sup> are great sources from which NCS solids are constructed with superior properties. However, inversion symmetry is often favorable during crystallization for its efficiency in close packing of the basic building units (BBUs),<sup>18,19</sup> and the challenges for synthesizing new NCS solids arises from aligning the FBUs without an inversion center. To direct an NCS structure, one efficient strategy is to introduce chiral BBUs since they do not possess an inversion center by nature. Solids with enantiomerically pure chiral BBUs are guaranteed to crystallize in the NCS chiral crystal classes because chiral BBUs with the same handedness can be related by proper symmetry operations

(translations, rotations, and combinations of these), but such solids often require enantiomeric purification, which complicates the synthetic process.

An alternative method to craft NCS solids with chiral BBUs is to combine enantiomers of both handedness and form racemates.<sup>20–22</sup> Although enantiomers with the opposite handedness can be related by an inversion center and crystallize into CS racemates, it is still possible to form NCS racemates with enantiomers of both handedness. Such formations requires the enantiomers to relate to one another by symmetry elements such as (i) mirror/glide planes, (ii) rotoinversions, (iii) dihedral rotations, and (iv) principle rotations (Figure 1).<sup>20,22</sup> When the enantiomers are related by mirror/glide planes or rotoinversion, the solid will form an

Received: May 23, 2023

Published: July 24, 2023



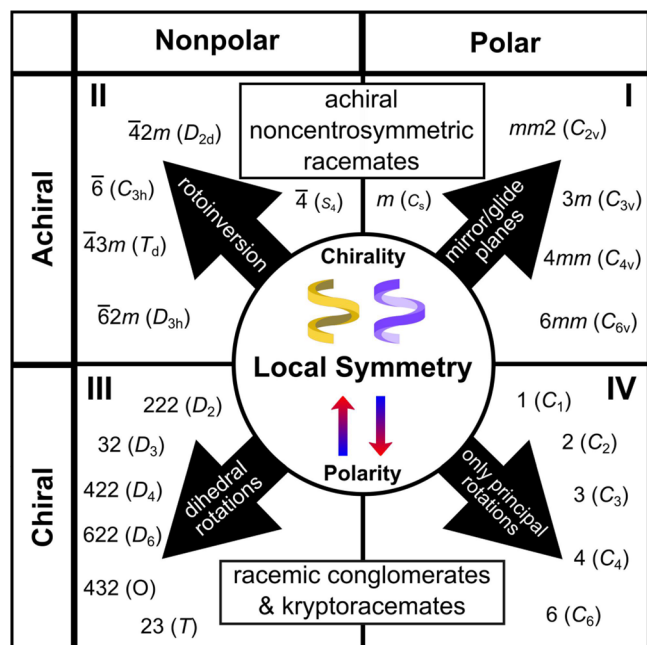


**Figure 1.** A roadmap for NCS racemates. Yellow and purple swirls represent enantiomers with opposite handedness, and the arrows represent the symmetry elements that relate the chiral BBUs.

achiral racemic compound, a single phase that is composed of equimolar enantiomers with the opposite handedness. When the enantiomers are related only by dihedral rotations and/or principle rotations, the solid will be chiral and form either racemic conglomerates—a mechanical mixture of enantiomeric crystals that each of crystal contains a single enantiomer<sup>24</sup>—or kryptoracemates—an extremely rare chiral crystal which contains enantiomers with opposite handedness that are symmetrically independent to each other.<sup>25,26</sup> In fact, it is not uncommon to find racemates in NCS crystals; for example, a manual screening of NCS organic crystals with mirror symmetry identified 632 racemates (16.5%) in the Cambridge Structural Database.<sup>27</sup> However, it still remains unclear how to break inversion symmetry between racemic BBUs at the molecular level, bringing challenges to designing new NCS racemates on a rational basis.<sup>28,29</sup>

Recently,  $\Delta/\Lambda\text{-Cu}(\text{bpy})_2(\text{H}_2\text{O})^{2+}$  complexes have been found to crystallize in the polar and achiral NCS space group  $Pna2_1$  with polar anions  $\text{MF}_6^{2-}$  ( $\text{M} = \text{Ti, Zr, Hf}$ ;  $\text{bpy} = 2,2'\text{-bipyridine}$ ).<sup>21,23</sup> Owing to second-order Jahn–Teller effects and hydrogen bonding network,  $\text{MF}_6^{2-}$  octahedra undergo an out-of-center distortion and are aligned by a screw axis, giving an overall polar moment. This NCS polar racemic structure (referred to as NCS-Cu/bpy/M hereafter) is unique and is one of the 4 NCS crystal structures out from 14 crystal structures that contain equimolar  $\Delta/\Lambda\text{-Cu}(\text{bpy})_2(\text{H}_2\text{O})^{2+}$  BBUs in the Cambridge Structural Database (CSD version 5.42 from March 2022), while the other NCS examples are compounds with multicomponent BBUs and complex motifs.<sup>30–32</sup> To further understand the chemical origins of inversion symmetry breaking in the NCS-Cu/bpy/M structure, we utilized bpy's derivatives with methyl substituents, dmbpy ( $\text{dmbpy} = 4,4'/5,5'\text{-dimethyl-2,2'\text{-bipyridine}}$ ) ligands, to perturb the coordination environment of the enantiomers and synthesized five new compounds with equimolar  $\Delta/\Lambda\text{-Cu}(\text{dmbpy})_2(\text{H}_2\text{O})^{2+}$  cations and  $\text{MF}_6^{2-}$  anions. We created a

series of structural descriptors to compare the structures and analyze the intermolecular interactions of the reported NCS and newly synthesized CS compounds. Through a detailed structural analysis, parallel heterochiral  $\pi\text{--}\pi$  interactions are identified as the key factor in the formation of the inversion center between adjacent Cu enantiomers, providing insights for the rational design of new NCS racemic materials.

## METHODS

**Caution:** Hydrofluoric acid (HF) is toxic and corrosive! HF must be handled with extreme caution and with the appropriate protective gear.

**Materials.**  $\text{TiO}_2$  (Aldrich, 99.9+%),  $\text{ZrO}_2$  (Alfa Aesar, 99.978%),  $\text{HfO}_2$  (Aldrich, 98%),  $\text{CuO}$  (SigmaAldrich,  $\geq 99.0\%$ ), 5,5'-dimethyl-2,2'-bipyridyl (Fisher Scientific,  $\geq 98.0\%$ ), 4,4'-dimethyl-2,2'-bipyridyl (SigmaAldrich, 99%), and HF(aq) (Sigma-Aldrich, 48 wt % in  $\text{H}_2\text{O}$ ,  $\geq 99.99+\%$  trace metals basis) were used as received. Reagent amounts of deionized water were used.

**Hydrothermal Synthesis.** The compounds reported here were synthesized via the hydrothermal pouch method.<sup>33</sup> In each reaction, the reagents were heat-sealed in Teflon pouches. Groups of six pouches were then placed into a 125 mL Parr autoclave with 40 mL of deionized water as backfill. The autoclave was heated at a rate of 5 °C/min to 150 °C and held at 150 °C for 24 h. The autoclaves were cooled to room temperature at a rate of 6 °C/h. Solid products were recovered via vacuum filtration.

Compound 1 [ $\text{Cu}(\text{Sdmbpy})_2(\text{H}_2\text{O})][\text{TiF}_6]\cdot\text{H}_2\text{O}$ ] was synthesized in a pouch containing 0.4195 mmol of  $\text{CuO}$ , 0.4195 mmol of  $\text{TiO}_2$ , 0.835 mmol of Sdmbpy, 0.05 mL (1.38 mmol) of HF(aq), and 0.2 mL (11 mmol) of  $\text{H}_2\text{O}$ . Greenish blue crystals (compound 1) were recovered by vacuum filtration with other unknown phases.

Compound 2 [ $\text{Cu}(\text{Sdmbpy})_2(\text{H}_2\text{O})][\text{ZrF}_6]\cdot1.5\text{H}_2\text{O}$ ] was synthesized in a pouch containing 0.4195 mmol of  $\text{CuO}$ , 0.4195 mmol of  $\text{ZrO}_2$ , 0.835 mmol of Sdmbpy, 0.15 mL (4.14 mmol) of HF(aq), and 0.1 mL (5.5 mmol) of  $\text{H}_2\text{O}$ . Greenish blue crystals (compound 2) were recovered by vacuum filtration with a small amount of other unknown phases.

Compound 3 [ $\text{Cu}(\text{Sdmbpy})_2(\text{H}_2\text{O})][\text{HfF}_6]\cdot1.09\text{H}_2\text{O}$ ] was synthesized in a pouch containing 0.4195 mmol of  $\text{CuO}$ , 0.4195 mmol of  $\text{HfO}_2$ , 0.835 mmol of Sdmbpy, 0.15 mL (4.14 mmol) of HF(aq), and 0.1 mL (5.5 mmol) of  $\text{H}_2\text{O}$ . Greenish blue crystals (compound 3) were recovered by vacuum filtration with a small amount of other unknown phases.

Compound 4 [ $\text{Cu}(\text{4dmbpy})_2(\text{H}_2\text{O})][\text{ZrF}_6]\cdot2.5\text{H}_2\text{O}$ ] was synthesized in a pouch containing 0.4195 mmol of  $\text{CuO}$ , 0.4195 mmol of  $\text{ZrO}_2$ , 0.835 mmol of 4dmbpy, 0.15 mL (4.14 mmol) of HF(aq), and 0.1 mL (5.5 mmol) of  $\text{H}_2\text{O}$ . Blue crystals (compound 4) were recovered by vacuum filtration with other unknown phases.

Compound 5 [ $\text{Cu}(\text{4dmbpy})_2(\text{H}_2\text{O})][\text{HfF}_6]\cdot1.09\text{H}_2\text{O}$ ] was synthesized in a pouch containing 0.4195 mmol of  $\text{CuO}$ , 0.4195 mmol of  $\text{HfO}_2$ , 0.835 mmol of Sdmbpy, 0.15 mL (4.14 mmol) of HF(aq), and 0.1 mL (5.5 mmol) of  $\text{H}_2\text{O}$ . Blue crystals (compound 5) were recovered by vacuum filtration with a small amount of other unknown phases.

**Single-Crystal X-ray Diffraction.** A suitable single crystal was mounted on a glass fiber with paratone oil, and the intensity data of the single crystal were collected at 100 K on an XtaLAB Synergy diffractometer equipped with a microfocus sealed X-ray tube PhotonJet (Mo) X-ray source and a Hybrid Pixel Array Detector (HyPix). Temperature of the crystal was controlled with an Oxford Cryosystems low-temperature device. Data reduction was performed with the CrysAlisPro software using a numerical absorption correction.<sup>34</sup> The structure was solved with the ShelXT,<sup>35</sup> using Intrinsic Phasing as implemented in Olex2.<sup>36</sup> The model was refined with ShelXL using least-squares minimization. The structures were checked for missing symmetry with PLATON.<sup>37</sup>

**Structural Descriptors.** In order to quantify the intermolecular interactions between the ligands in the Cu complexes, we have introduced the following descriptors adopted from a published work

by Petrović et al.<sup>38</sup> The stacking interactions between the adjacent bpy ligands can appear between C<sub>5</sub>N-aromatic rings and are described with distances  $d_{pp}$ ,  $R$ , and  $r_{mm}$  (Figure 2a) and torsion angles  $T_1$

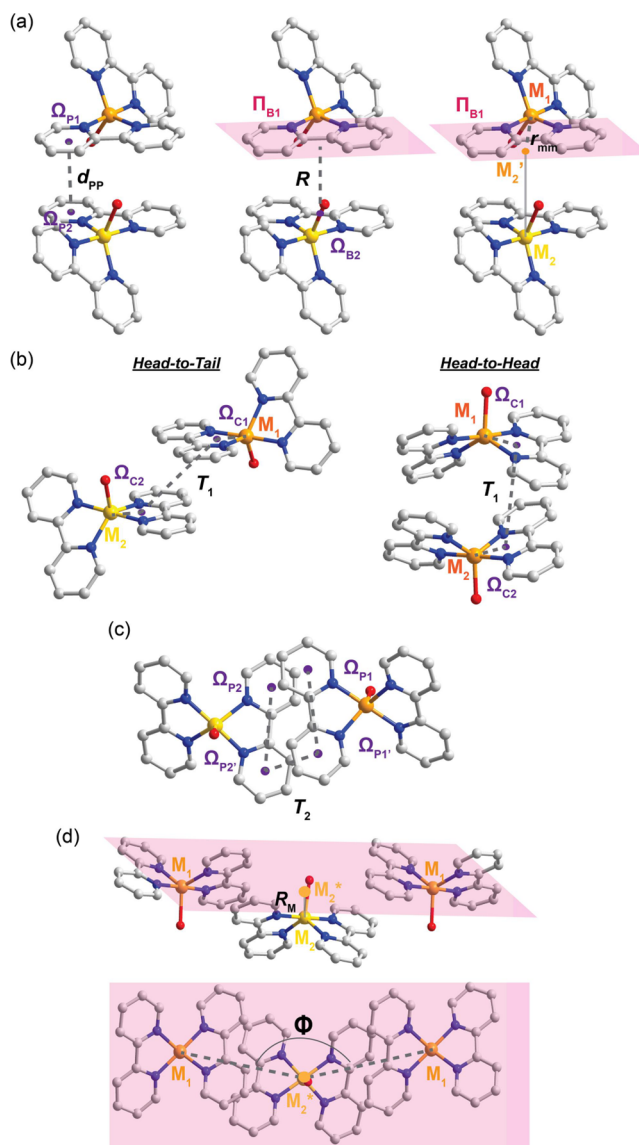


**Figure 2.** Illustration of descriptors (a) distance  $d_{pp}$  (left),  $R$  (middle), and  $r_{mm}$  (right) and torsion angles (b)  $T_1$  and (c)  $T_2$ . (d) Illustration of descriptor distance  $R_M$  (top) and angle  $\Phi$  (bottom). The examples are taken from the reported compound  $[\text{Cu}(\text{H}_2\text{O})\text{-bpy}]_2[\text{TiF}_6]\cdot 2\text{H}_2\text{O}$ .

(Figure 2b) and  $T_2$  (Figure 2c). The three distances represent the displacements of the interacting ligands in the three directions. Distance  $d_{pp}$  is the shortest distance between centroids of two pyridine fragments ( $\Omega_{P1}$  and  $\Omega_{P2}$ ) from the adjacent interacting ligands. Distance  $R$  is the distance from the centroid of the ligand of the second complex ( $\Omega_{B2}$ ) to the average plane including the interacting ligand of the first complex ( $\Pi_{B1}$ ). Distance  $r_{mm}$  is the distance from the metal ion of the first complex ( $M_1$ ) to the projection of the metal ion of the second complex onto  $\Pi_{B1}$  ( $M_2'$ ). Torsion angle  $T_1$  represents the relative direction of the interacting ligands. Torsion angle  $T_1$  is defined as the  $M_1-\Omega_{C1}-\Omega_{C2}-M_2$  angle, and  $\Omega_{C1}$  and  $\Omega_{C2}$  are defined as the centroids of the chelate rings from the first and second complexes, respectively. When  $T_1$  falls between  $0^\circ$  and  $90^\circ$ , the two interacting ligands tend to head in the same direction and are head-to-head oriented. Otherwise, when  $T_1$  falls

between  $90^\circ$  and  $180^\circ$ , the two interacting ligands tend to head in opposing directions and are head-to-tail oriented. Torsion angle  $T_2$  represents the stacking arrangements between the interacting ligands and is defined as the  $\Omega_{P1}-\Omega_{P1'}-\Omega_{P2}-\Omega_{P2'}$  angle. If  $T_2$  is smaller than  $90^\circ$ , it indicates that both C<sub>5</sub>N-aromatic rings from the ligands overlap, and conversely, if  $T_2$  is larger than  $90^\circ$ , it indicates that only one C<sub>5</sub>N-aromatic ring from each ligand overlap. When  $T_2$  is  $0^\circ$  or  $180^\circ$ , the two ligands are aligned parallel and their geometry corresponds to parallel packing. Otherwise, the two ligands are aligned with an angle, and their geometry corresponds to nonparallel packing.

To describe the arrangement of the Cu enantiomers in the racemic chains of the compounds discussed, we developed two descriptors,  $R_M$  and  $\Phi$  parameters, for measuring the offset of BBUs (Figure 2d). Distance  $R_M$  is the normal distance from the Cu atom of the enantiomer with up orientation ( $M_2$ ) to the average plane including all the Cu atoms of the enantiomer with down orientation ( $M_1$ ) in a certain racemic chain. The angle  $\Phi$  is defined as  $M_1-M_2^*-M_1$  where  $M_2^*$  is the projection of  $M_2$  onto the average plane of  $M_1$ . The  $R_M$  and  $\Phi$  parameters present the offsets of the racemates perpendicular to and along the chain direction.

## RESULTS

**Structure Descriptions.** In order to investigate how steric effects influence racemates' crystal packing, we introduced methyl groups on 2,2'-bipyridyl ligands and examined two distinct substituent positions where one is on the 5,5'-position while the other is on the 4,4'-position. By exploring the synthesis of CuO, MO<sub>2</sub>/dmbpy/HF(aq) (M = Ti, Zr, Hf; dmbpy = 4,4'-dimethyl-2,2'-dipyridyl, 5,5'-dimethyl-2,2'-dipyridyl), we discovered three compounds based on racemic combinations of  $\Delta/\Lambda\text{-Cu}(\text{5dmpy})_2(\text{H}_2\text{O})^{2+}$  cations and  $\text{MF}_6^{2-}$  anions (namely, compounds **1**, **2**, and **3**) and two compounds based on combinations of chiral  $\Delta/\Lambda\text{-Cu-(4dmpy)}_2(\text{H}_2\text{O})^{2+}$  cations and  $\text{MF}_6^{2-}$  anions (namely, compounds **4** and **5**). The crystallographic information is summarized in Tables S1 and S2.

Compound **1** has the formula  $[\text{Cu-(5dmbpy)}_2(\text{H}_2\text{O})_2][\text{TiF}_6] \cdot 2\text{H}_2\text{O}$  and crystallizes in space group  $P1$ . The asymmetric unit of **1** contains two chiral  $\text{Cu}(\text{5dmbpy})_2(\text{H}_2\text{O})^{2+}$  cations with the same handedness but different orientations, two positionally disordered  $\text{TiF}_6^{2-}$  anions, and two free water molecules with one being positionally disordered. The Cu enantiomers with the opposite handedness ( $\Delta u/\Delta d$  and  $\Delta d/\Delta u$ ) are generated by an inversion center, and the two sets of racemic  $\Delta/\Lambda\text{-Cu}(\text{5dmbpy})_2(\text{H}_2\text{O})^{2+}$  cations display  $C_2$  symmetry. The angle between the copper atom and centroids of the two ligands in the cations is slightly different between the two sets, with one being  $141.01^\circ$  and the other being  $137.15^\circ$  (Figure S1). To examine the geometry of the cations, the  $\tau_5$  parameter  $(\tau_5 = \frac{\beta - \alpha}{60^\circ})$  was used where  $\beta$  and  $\alpha$  represent the largest and second largest bond angles.<sup>39</sup> The value of the  $\tau_5$  parameter indicates the shape of the five-vertex polyhedron formed by the molecule; when  $\tau_5 = 0$ , the shape is a square pyramid, while  $\tau_5 = 1$  indicates a triangular bipyramidal. For the Cu cations in **1**,  $\tau_5$  values are 0.90/0.87, indicating that the shapes of the cations are close to triangular bipyramidal. Two racemic chains are formed via heterochiral  $\pi-\pi$  stacking interactions between Cu enantiomers with opposite handedness and run along the  $c$  axis with the arrangements of  $\Delta d-\Delta u-\Delta d-\Delta u$  and  $\Delta u-\Delta d-\Delta u-\Delta d$  ( $u = \text{up}$  and  $d = \text{down}$  describe the orientation of these cations along the  $b^*$  direction). Then, the chains are extended into layers by altering the arrangements and stacking

Cu enantiomers with the same handedness via homochiral  $\pi$ – $\pi$ -stacking interactions (Figure 3a). The  $\text{TiF}_6^{2-}$  anions are

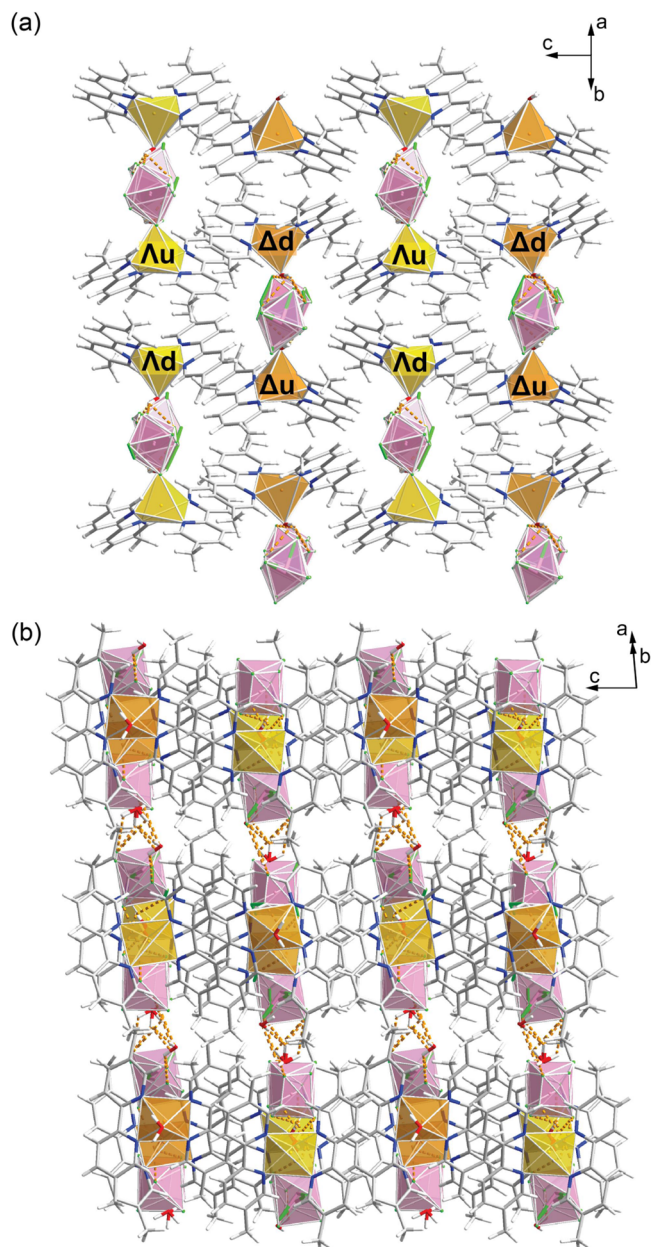


**Figure 3.** (a) Racemic layer of **1** view against the  $c$  axis. (b) Crystal structure of **1** view against the  $c$  axis (this view is produced from Figure 3a by 90° rotation around the horizontal direction). Orange, blue, red, gray, and white spheres represent Cu, N, O, C, and H atoms, respectively. Yellow, orange, and pink polyhedra represent Cu-centered cations with  $\Lambda$ - and  $\Delta$ -configurations and Ti-centered anions, respectively. The orange dashed line represent hydrogen bonds.

in the voids created within layers of homochiral enantiomers, forming hydrogen bonds with the bound water on the cations. Each  $\text{TiF}_6^{2-}$  anion participates in hydrogen bonding with ligated water on two Cu enantiomers of the same handedness, and as a result, Ti–F bond lengths vary from 1.831(2) to 1.908(3) Å. The differences in bond lengths lead to a small out of center distortion in the  $\text{TiF}_6^{2-}$  octahedron, but the overall centrosymmetry of the crystal cancels the polar moment

between  $\text{TiF}_6^{2-}$  anions. Finally, the layers stack in three dimensions in an eclipsed manner through a weaving-shaped intermolecular hydrogen bond network between the  $\text{TiF}_6^{2-}$  anions and free waters (Figure 3b).

Compound **2** has the formula  $[\text{Cu}(\text{SdmBPy})_2(\text{H}_2\text{O})]_2[\text{ZrF}_6]_2 \cdot 2.5\text{H}_2\text{O}$  and crystallizes in space group  $P1$ . Similar to **1**, the asymmetric unit of **2** also contains two  $\text{Cu}(\text{SdmBPy})_2(\text{H}_2\text{O})^{2+}$  cations with the same handedness but different orientations, two  $\text{ZrF}_6^{2-}$  anions, and three free water molecules; all the anions and the free water molecules are positionally ordered in **2**. The Cu cations in **2** also appear with  $C_2$  symmetry, with the angles between the Cu atom and the centroids of ligands being 150.90° and 145.26° (Figure S2). The calculated  $\tau_s$  values are 0.83 and 0.80 for each independent Cu cation in **2**, indicating a triangular bipyramidal geometry for both. The  $\text{ZrF}_6^{2-}$  anions connect to the free water and the bound water of Cu cations through hydrogen bonding, giving rise to slightly distorted octahedra with Zr–F bond lengths varying from 1.9887(13) to 2.0235(12) Å. The overall dipole moment of the anions is counteracted by the centrosymmetry of the crystal. The layer packing pattern of **2** is comparable to **1**. Cu enantiomers with the opposite handedness arrange in  $\Lambda d$ – $\Delta u$ – $\Lambda d$ – $\Delta u$  and  $\Lambda u$ – $\Delta d$ – $\Lambda u$ – $\Delta d$  chains ( $u$  = up and  $d$  = down) describe the orientation of these cations along the  $b$  direction) along the  $c$  axis via heterochiral  $\pi$ – $\pi$  stacking interactions, and the chains pack into layers along the  $b$  axis via homochiral  $\pi$ – $\pi$  stacking (Figure 4a). The disparity between **1** and **2** is interlayer stacking. In **2**, a different weaving-shaped hydrogen bonding network leads to an interlayer architecture in a staggered manner rather than an eclipsed manner along the  $a$  axis (Figure 4b).

Compound **3** has the formula  $[\text{Cu}(\text{SdmBPy})_2(\text{H}_2\text{O})]_2[\text{HfF}_6]_2 \cdot 2.1\text{H}_2\text{O}$  and is isostructural with **2** except for slightly different free water positions and occupancies. The angles between the Cu atom and the centroids of the ligands are 149.19/145.13°, and  $\tau_s$  values for the Cu complexes are 0.83/0.84 in **3**. The anions are minorly distorted and Hf–F bond lengths vary from 1.970(3) to 2.019(3) Å.

Compound **4** has the formula  $[\text{Cu}(\text{4dmBPy})_2(\text{H}_2\text{O})]_2[\text{ZrF}_6]_2 \cdot 7\text{H}_2\text{O}$  and crystallizes in space group  $P2_1/c$ . Similar to the aforementioned compounds, the asymmetric unit of **4** contains two  $\text{Cu}(\text{4dmBPy})_2(\text{H}_2\text{O})^{2+}$  cations with the same handedness but different orientations, two unique  $\text{ZrF}_6^{2-}$  anions, and five free water molecules. However, the symmetry of the Cu cations is reduced to  $C_1$  owing to the large tilt of the apical bound water ligand. Similar symmetry reduction in five-coordinated Cu complexes were also reported in compounds with  $\text{Cu}(\text{phen})_2(\text{H}_2\text{O})^{2+}$  cations and  $\text{Cu}(\text{phen})_2\text{MF}_6$  ( $\text{phen}$  = 1,10-phenanthroline;  $M$  = Zr, Hf) molecules.<sup>40,41</sup> In addition, the angles between the Cu atom and centroids of the ligands are quite different between the two unique cations, with Cation 1 being 151.41° and Cation 2 being 169.82° (Figure 5a). Notably, the angle in Cation 2 is distinctly larger than the rest of cations in this study. The  $\tau_s$  values of Cu cations in **4** are 0.55/0.46, indicating that the shape of the cations is largely distorted and cannot be described as either a triangular bipyramidal or a square pyramid. Interestingly, the second largest angle  $\beta$  is O1–Cu1–N3 for Cation 1 while it is –6–Cu2–N8 for Cation 2, suggesting that the bound water in Cation 1 is more tilted. Nevertheless, the distortion in the cations does not pose a large influence on the

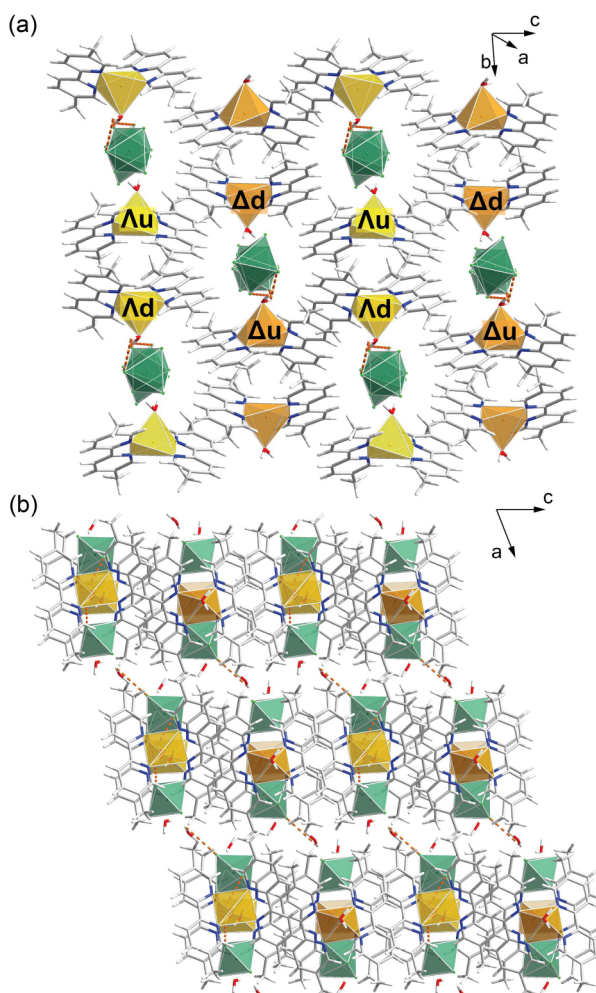


**Figure 4.** (a) Racemic layer of compound 2 in the  $bc$  plane. (b) Crystal structure of compound 2 viewed along the  $b$  axis. Orange, blue, red, gray, and white spheres represent Cu, N, O, C, and H atoms, respectively. Yellow, orange, and green polyhedra represent Cu-centered cations with  $\Lambda$ - and  $\Delta$ -configuration and Zr-centered anions, respectively. The orange dashed line represents hydrogen bonds.

enantiomer stacking, and the Cu enantiomers still pack into  $\Lambda$ d– $\Delta$ u– $\Lambda$ d– $\Delta$ u and  $\Lambda$ u– $\Delta$ d– $\Lambda$ u– $\Delta$ d chains along the  $c$  axis ( $u$  = up and  $d$  = down describe the orientation of these cations along the  $a$  direction) via heterochiral  $\pi$ – $\pi$  stacking interactions and extend into layers via homochiral  $\pi$ – $\pi$  stacking interactions. Moreover, the pair of enantiomers with opposite handedness ( $\Lambda$ u/ $\Delta$ d and  $\Lambda$ d/ $\Delta$ u) is still related by an inversion center along the chain. The distortion in the cations leads to a tilt on the chain stacking, giving the  $\beta$  angle a value of  $96.078(2)^\circ$  (Figure 5b). Different from compounds 1, 2, and 3, the two unique anions in 4 are not evenly distributed on the sides of the layers. In 4, Anion 1 occupies the voids created by the adjacent racemic chains within the layer, while Anion 2 is positioned between the layers. The uneven distribution of anion complicates the hydrogen bonding network wherein both anions form hydrogen bonds with cation 1 but only anion 1 forms hydrogen bonds with cation 2. Despite the different hydrogen bonding schemes, the  $\text{ZrF}_6^{2-}$  octahedra are similar to those in 2, with  $\text{Zr}$ – $\text{F}$  bond lengths ranging from  $1.972(2)$  to  $2.0345(19)$  Å. The layers stack into three dimensions in an eclipsed manner through a linear intermolecular hydrogen bond network, where the free water molecules between the layers only form a hydrogen bond with anion 2 (Figure 5c).

Compound 5 has the formula  $[\text{Cu}-(4\text{dmBPy})_2(\text{H}_2\text{O})]_2[\text{HfF}_6]_2 \cdot 7\text{H}_2\text{O}$  and is isostructural with compound 4. The cations in 5 are also distorted and tilted with the angle between the Cu atom and centroids of the ligands being  $151.4^\circ/169.84^\circ$  and  $\tau_5$  values being  $0.55/0.47$ . The  $\text{Hf}$ – $\text{F}$  bond lengths vary from  $1.9668(19)$  to  $2.0262(18)$  Å.

**Structural Descriptors for  $\pi$ – $\pi$  Interactions.** Single crystal X-ray diffraction reveals three new structure types in compounds 1–5. Unlike the reported NCS-Cu/bpy/M structure, all compounds in this work crystallize in CS space groups, even though they share similar packing motifs. To understand the nuance of packing patterns, we investigate the  $\pi$ – $\pi$  stacking interactions between the adjacent Cu enantiomers in the reported NCS compounds and compounds 1–5 using the descriptors defined in the Methods section. The five descriptors,  $d_{\text{pp}}$ ,  $R$ ,  $r_{\text{mm}}$ ,  $T_1$ , and  $T_2$ , depict the geometry of  $\pi$ – $\pi$  stacking interactions between enantiomers in different aspects. The  $d_{\text{pp}}$  and  $R$  parameters describe the direct and normal

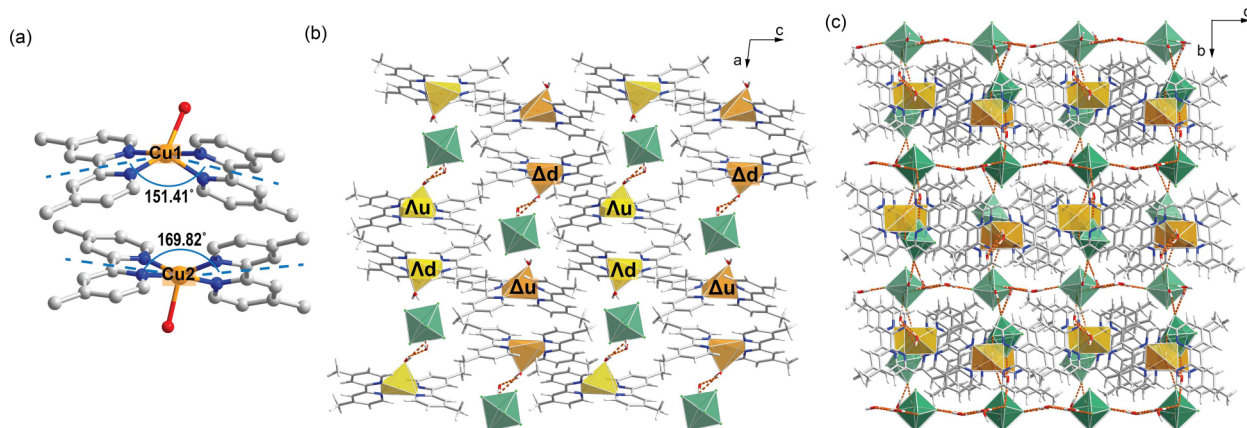


**Figure 5.** (a) Representation of the two  $\Delta$ -Cu(4dmBPy)<sub>2</sub>(H<sub>2</sub>O)<sup>2+</sup> enantiomers in the asymmetric unit of 4. Hydrogen atoms are omitted. (b) Racemic layer of 4 view along the  $b$  axis. (c) Crystal structure of 4 view along the  $a$  axis. Orange, blue, red, gray, and white spheres represent Cu, N, O, C, and H atoms, respectively. Yellow, orange, and green polyhedra represent Cu-centered cations with  $\Lambda$ - and  $\Delta$ -configuration and Zr-centered anions, respectively. The orange dashed line represents hydrogen bonds.

distance between the interacting aromatic rings, respectively, while the  $r_{mm}$  parameter indicates the overlaps between the chelate–chelate stacking interactions. The two torsion angles,  $T_1$  and  $T_2$ , determine the orientation of the chelate rings and the relative direction of the interacting aromatic rings, respectively. A  $T_1$  angle smaller than  $90^\circ$  corresponds to a head-to-head orientation, while a  $T_1$  angle larger than  $90^\circ$  corresponds to a head-to-tail orientation. The absolute value of  $|T_2|$  suggests the deviation between the directions of the interacting ligands.

The resulting descriptor values are provided in Tables S3–S5 and both heterochiral (along the chain direction) and homochiral (against the chain direction)  $\pi$ – $\pi$  stacking interactions are examined. For each NCS-Cu/bpy/M compound, two unique heterochiral and two unique homochiral  $\pi$ – $\pi$  stacking interactions are found. For each CS compound, four unique heterochiral and two unique homochiral  $\pi$ – $\pi$ -stacking interactions are found. Among the measured heterochiral  $\pi$ – $\pi$  stacking interactions, the values of the  $R$  parameter vary little across different compounds and are all in a range of 3.221–3.725 Å, suggesting that the normal distance between the interacting aromatic rings does not change significantly between the NCS and CS compounds. In compounds 4 and 5,  $d_{pp}$  and  $r_{mm}$  range between 6.1 and 10.6 Å, respectively, which are significantly larger than the values in the rest of the other compounds (Figure 6a). The deviation is due to the low symmetry and large distortion of the  $\text{Cu}(4\text{dmbpy})_2(\text{H}_2\text{O})^{2+}$  complex, leading to uneven spacing between the Cu enantiomers in the chain, as every other Cu enantiomer is closer to one neighbor and further away from the other (Figure S3). Interestingly, the extreme  $d_{pp}$  and  $r_{mm}$  values are only found in the racemic chains containing cation 2 and might be influenced by other secondary molecular forces such as hydrogen bonding. Among the measured homochiral  $\pi$ – $\pi$  stacking interactions, the values of the  $R$ ,  $d_{pp}$ , and  $r_{mm}$  parameters are in the ranges of 3.348–4.074, 3.815–4.453, and 2.188–4.206 Å with no distinct outlier.

The values of the  $T_1$  and  $T_2$  parameters found in the heterochiral  $\pi$ – $\pi$  stacking interactions are in the ranges of 165–180° and 0–10°, respectively, suggesting that the chelate rings are in a head-to-tail orientation and both aromatic rings overlap along the chain (Figure 6b). Notably, the values of the  $T_1$  and  $T_2$  parameters are exactly 180° and 0° for all the CS compounds 1–5 while they vary between 165.95 and 172.27° in the NCS-Cu/bpy/M compounds. This fact manifests a distinct nuance of the comparable packing patterns between CS and NCS compounds, in which the heterochiral  $\pi$ – $\pi$  interactions are parallel between the adjacent pair of enantiomers with opposite handedness in the CS structures but are nonparallel in the NCS structure. For the homochiral  $\pi$ – $\pi$  stacking interactions, the  $T_1$  parameter and the  $T_2$  parameter are in the ranges 0.17–28.43° and 3.01–19.55°, suggesting a head-to-head and nonparallel orientation. No obvious trend is found in the homochiral  $\pi$ – $\pi$  stacking interactions.

**Structural Descriptors for Racemic Chain Arrangement.** To probe the nuance of chain arrangements between the NCS and CS compounds, we utilized the  $R_M$  and  $\Phi$  descriptors, and the results are summarized in Tables S6–S8. The  $R_M$  parameter describes the normal distance between the enantiomers with opposite handedness along the chains, and the  $\Phi$  parameter depicts the offset degree of the racemic chains. Regardless of the space group the compound

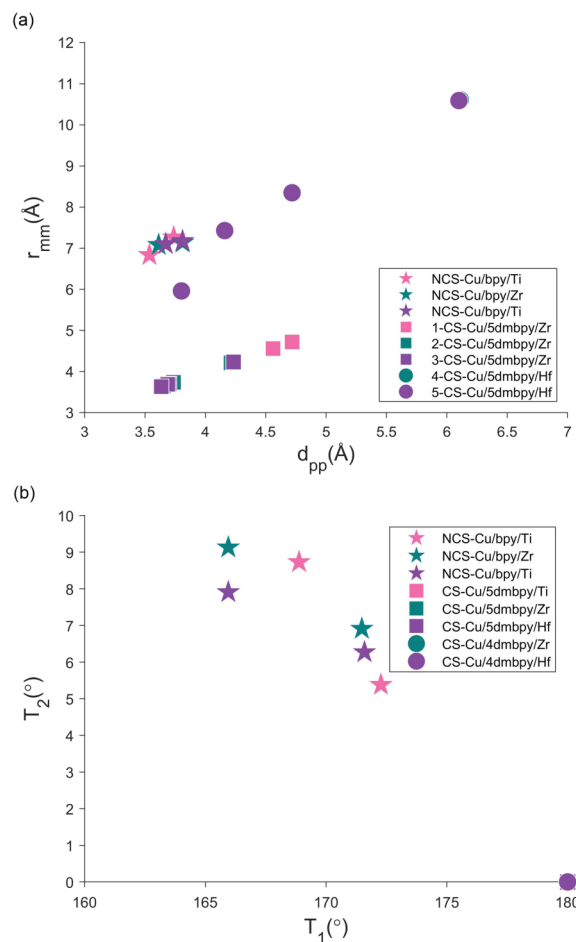


**Figure 6.** Summary of (a)  $d_{pp}$ ,  $r_{mm}$ , (b)  $T_1$  and  $T_2$  parameters for heterochiral  $\pi$ – $\pi$  stacking interactions in the reported NCS compounds and compounds 1–5. The pink, green, and purple squares are eclipsed in (b).

crystallizes in, the chain of each structure features a zigzag pattern. The results of the  $R_M$  parameters give similar values in most of the compounds, and the outlier appears in one of the chain compounds 4 and 5 (Figure S3). The large  $R_M$  values in this chain can be rationalized by the flat geometry of Cation 2, giving a distinct offset in the packing of the enantiomers. The results of the  $\Phi$  parameters give values ranging from 151.40 to 178.10°. It indicates that the enantiomers in the chains are fluctuating in different levels. The chains that have the largest  $\Phi$  parameters with a nearly linear shape is the chains containing Cu1 in compounds 2 and 3. There is no clear trend to distinguish NCS and CS compounds based on the chain arrangement.

## ■ DISCUSSION

**Nonparallel  $\pi$ – $\pi$  Interactions Break Local Inversion Symmetry between Racemates.** The analysis of structural descriptors for  $\pi$ – $\pi$  interactions highlights a clear distinction between the NCS and CS racemic compounds, which is the manner of stacking racemic BBUs. In the CS structures, the ligands of enantiomeric pairs stack in parallel while in the NCS structures they stack in nonparallel conformations (Figure 7). Moreover, the inversion center appears exactly in the center of the parallel heterochiral  $\pi$ – $\pi$  interactions between the adjacent pair of enantiomers (eg:  $\Delta u\text{-Cu1}/\Delta d$ -

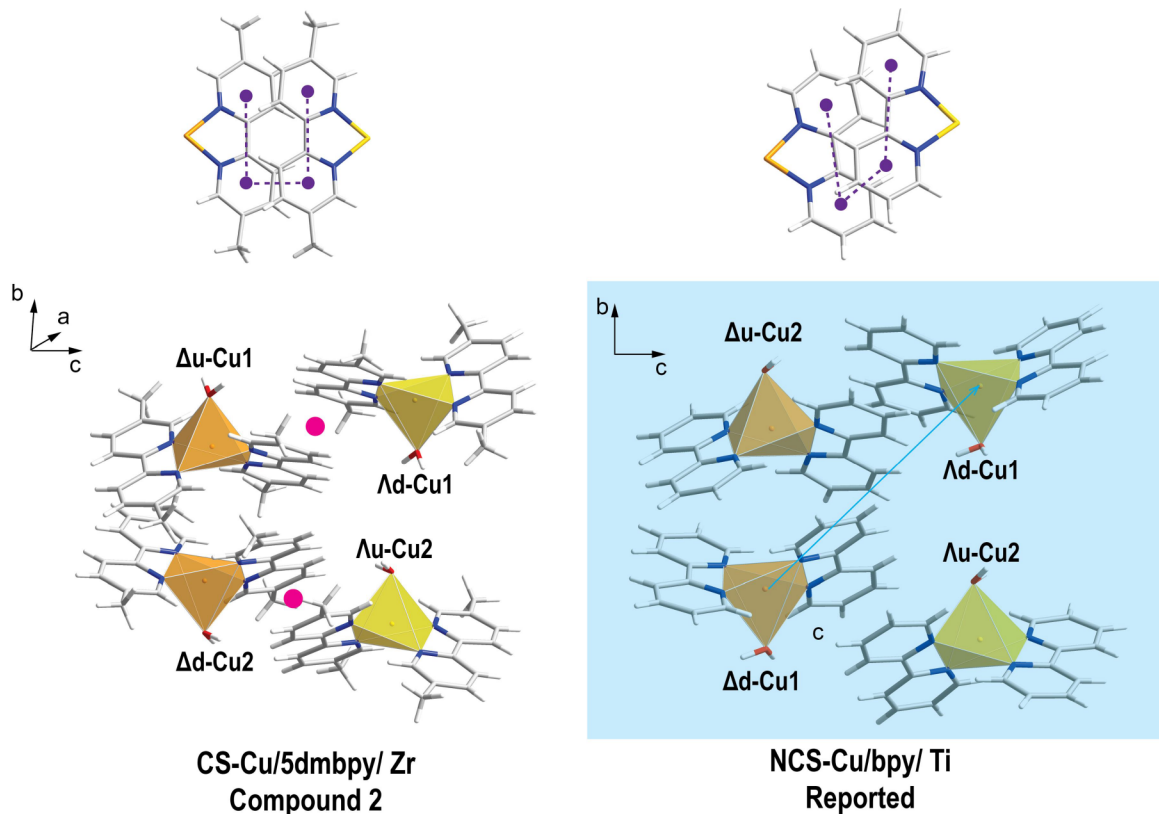


**Figure 7.** Parallel and nonparallel heterochiral  $\pi$ – $\pi$ -stacking interactions in NCS and CS compounds. The  $T_2$  descriptor (top) and symmetry operations related to the enantiomers with opposite handedness (bottom) are labeled. The pink circles and blue plane/arrow represent the inversion center and  $n$  glide, respectively.

Cu1) along the chain in the CS structures (Figure 7). Contrastingly, in the NCS structure, no symmetry element relates to the adjacent pair of enantiomers (eg:  $\Delta u$ -Cu2/ $\Delta d$ -Cu1) along the chain owing to the nonparallel heterochiral  $\pi$ – $\pi$  stacking, and the enantiomers with opposite handedness (eg:  $\Delta d$ -Cu1/ $\Delta u$ -Cu1) are related by an  $n$  glide plane across the chains (Figure 7). The parallel heterochiral  $\pi$ – $\pi$  stacking interactions in compounds 1–5 can be explained by the steric effect of the methyl groups on the ligands, in that the bulk methyl groups favors parallel stacking to minimize free volume.<sup>19</sup> Similar parallel heterochiral  $\pi$ – $\pi$  packings were observed in racemic compounds with other methyl-substituted ligands and the aromatic ligand 1,10-phenanthroline, and an inversion center is always found between the racemates.<sup>40,42,43</sup> As a result, although the asymmetric unit of the discussed compounds contains equivalent BBUs, the BBUs are related by different symmetry elements, resulting in different extended structures. The racemic chains display a similar pattern but have different compositions between the NCS and CS structures. In the NCS structure, two unique racemic BBUs are running along the chain, e.g.:  $\Delta u$ -Cu2– $\Delta d$ -Cu1– $\Delta u$ -Cu2– $\Delta d$ -Cu1, but in the CS structures, the chain only contain one unique BBU, e.g.:  $\Delta u$ -Cu1– $\Delta d$ -Cu1– $\Delta u$ -Cu1– $\Delta d$ -Cu1 (Figure 7).

While the current study details that parallel stacking interactions lead to a centrosymmetric arrangement of racemic motifs and that nonparallel stacking interactions leads to a noncentrosymmetric arrangement of racemic motifs, it cannot be said that the occurrence of parallel or nonparallel stacking interactions defines the presence of an inversion center. It has yet to be observed by the authors if there are instances of

parallel heterochiral  $\pi$ – $\pi$  stacking interactions in NCS racemates, although in the case of the compounds in this work, the nonparallel stacking interactions are necessary for inversion symmetry breaking. Furthermore, while in the CS compounds with parallel stacking interactions, the inversion center was found between the enantiomeric pair within the chain; this is not the only location that an inversion center can be located within the structure or the only way the enantiomeric pair can be related to one another.

**Hydrogen Bonding Network Leads to Different Interlayer Structures.** Apart from the  $\pi$ – $\pi$  stacking interactions, hydrogen bonding also plays a very important role in constructing the racemic structure, especially in interlayer stacking. We analyzed the hydrogen bonding interactions across the discussed compounds and found that the geometry of the Cu enantiomer is strongly related to the local hydrogen bonding network. As shown in Figure S4, because of different distributions of free water, the  $\text{MF}_6^{2-}$  octahedra displays slightly different orientations across the NCS compounds and compounds 1–3. It gives rise to a slight offset in the relative positions of the Cu enantiomers across the chain and a small tilt on the chain packing. The deviated hydrogen bonding network in compounds 4–5 derives from the unique voids created by the 4dmbpy ligands, which lead to the uneven distribution of the anions (Figure S5). The asymmetric anion distribution induces large distortion of the  $\text{Cu}(4\text{dmbpy})_2(\text{H}_2\text{O})^{2+}$  cations and thereby reduces the symmetry of the cations to  $C_1$ . The unique anion arrangements and linear hydrogen bonding network exclude an inversion center between the layers, and the adjacent layers are related by a glide plane and screw axis in compounds 4–5. While in

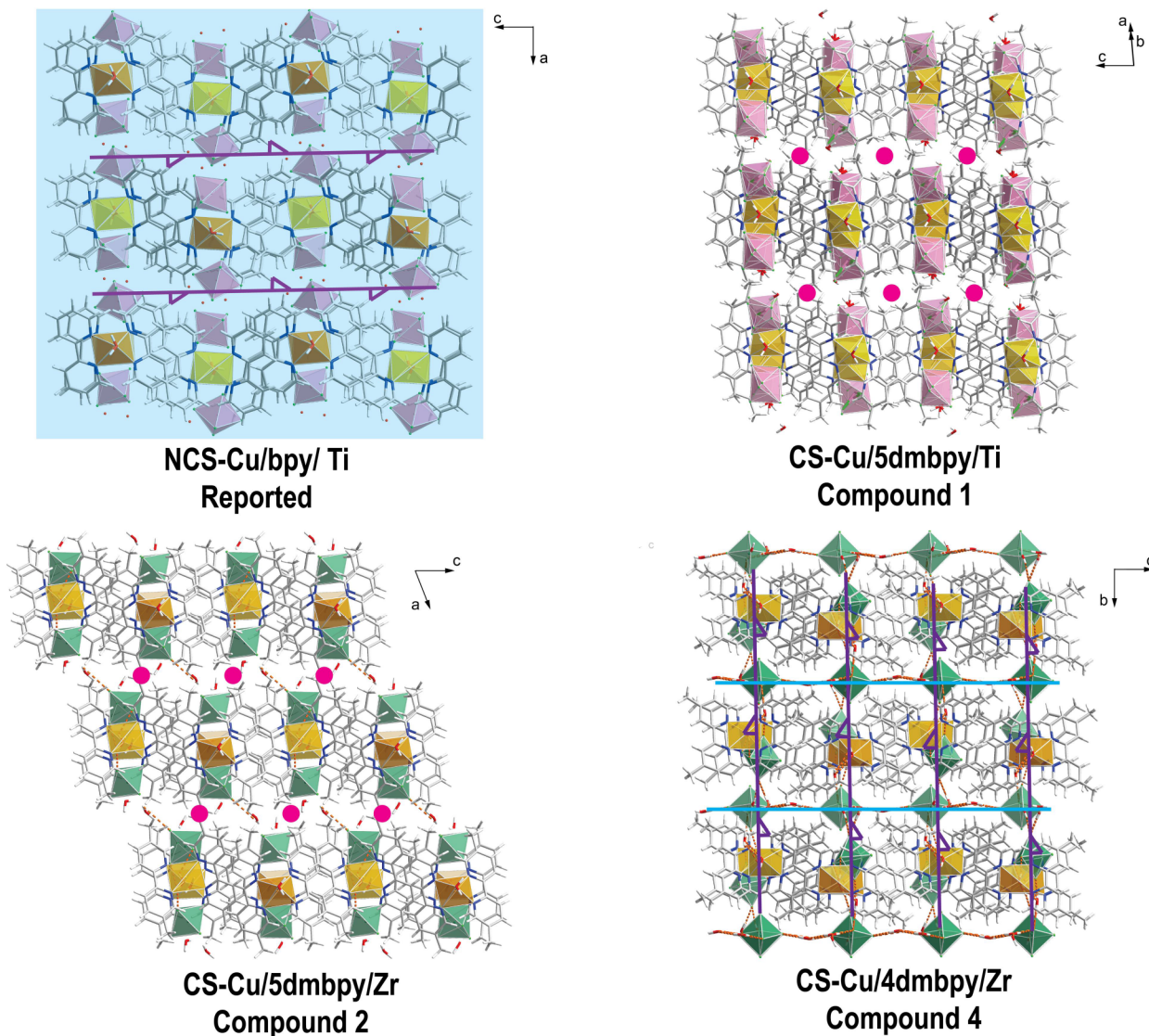


**Figure 8.** Interlayer architectures in the discussed compounds. Orange dashed line represents hydrogen bonding. The blue, pink, and purple labels represent the glide plane, inversion center, and screw axis, respectively.

compounds 1–3, evenly distributed anion arrangements and intricate hydrogen bonding networks produce an inversion symmetry between the layers (Figure 8). Note that although NCS compounds and compounds 1–3 present similarities in the anion arrangements and hydrogen bonding networks, the methyl group in compounds 1–3 enables a larger void and increased interlayer distance for the anions to align in a preferred orientation that minimizes the net dipole moment so that the layers are packed through an inversion center other than a screw axis in NCS compounds (Figure 8).

## CONCLUSIONS

In summary, we synthesized five new CS racemic compounds with dmbpy ligands and structurally analyzed their intermolecular forces in comparison with previously reported NCS racemic compounds. The structural descriptors have demonstrated that all CS compounds display parallel heterochiral  $\pi$ – $\pi$  interactions between the adjacent enantiomers, despite the difference in interlayer architecture, hydrogen bonding network, and cation geometry. In contrast, all heterochiral  $\pi$ – $\pi$  interactions in the NCS compounds are nonparallel, which

breaks the inversion center between the adjacent enantiomers. The parallel heterochiral  $\pi$ – $\pi$  stacking in the compounds with dmbpy ligands can be explained by steric effects of the methyl group. Altogether, we demonstrate that nonparallel packing of ligands plays a very important role in breaking inversion symmetry between enantiomers, and racemic BBUs which favor nonparallel packing have great potential to form NCS racemates.

Furthermore, through the structural analysis of the five newly synthesized compounds and the comparison of these to the related NCS phases, common symmetry elements related to enantiomeric pairs and their resulting space groups (Figure 1) have been identified. Ongoing work is focused on a comprehensive computational search for racemates in the NCS achiral crystal classes. Through this, we aim to unlock more secrets behind inversion symmetry breaking in racemates, which will provide further synthetic guides, such as desirable racemic BBUs, to target racemic materials with superior NCS properties. This goal aligns well with that outlined by A. F. Wells almost 70 years ago in 1956, “to encourage the reader to think ‘in three dimensions’ so that he will come to regard the

formation of three-dimensional arrangements of atoms in crystals as the logical results of the same processes that lead to the more familiar finite groups of atoms of ordinary chemical experience.”<sup>44</sup>

## ■ ASSOCIATED CONTENT

### ■ Supporting Information

The Supporting Information is available free of charge at <https://pubs.acs.org/doi/10.1021/jacs.3c05380>.

Crystallographic tables for compounds 1–5; tables of structural descriptors for  $\pi$ – $\pi$  stacking interactions for compounds 1–5; additional structural figures of chain and cation arrangements; and figures of hydrogen bonding networks (PDF)

### Accession Codes

CCDC 2264645, 2264646, 2264647, 2264648, and 2264649 contains the supplementary crystallographic data for this paper. These data can be obtained free of charge via [www.ccdc.cam.ac.uk/data\\_request/cif](http://www.ccdc.cam.ac.uk/data_request/cif), or by emailing [data\\_request@ccdc.cam.ac.uk](mailto:data_request@ccdc.cam.ac.uk), or by contacting The Cambridge Crystallographic Data Centre, 12 Union Road, Cambridge CB2 1EZ, UK; fax: +44 1223 336033.

## ■ AUTHOR INFORMATION

### Corresponding Author

**Kenneth R. Poeppelmeier** – Department of Chemistry, Northwestern University, Evanston, Illinois 60208, United States;  [orcid.org/0000-0003-1655-9127](https://orcid.org/0000-0003-1655-9127); Email: [krp@northwestern.edu](mailto:krp@northwestern.edu)

### Authors

**Yiran Wang** – Department of Chemistry, Northwestern University, Evanston, Illinois 60208, United States;  [orcid.org/0000-0002-3642-2294](https://orcid.org/0000-0002-3642-2294)

**Matthew L. Nisbet** – Department of Chemistry, Northwestern University, Evanston, Illinois 60208, United States

**Kendall R. Kamp** – Department of Chemistry, Northwestern University, Evanston, Illinois 60208, United States;  [orcid.org/0000-0003-2715-1514](https://orcid.org/0000-0003-2715-1514)

**Emily Hiralal** – Department of Chemistry, Northwestern University, Evanston, Illinois 60208, United States

**Romain Gautier** – Institut des Matériaux Jean Rouxel (IMN), Université de Nantes, CNRS, Nantes cedex 3 F-44000, France

**P. Shiv Halasyamani** – Department of Chemistry, University of Houston, Houston, Texas 77204-5003, United States;  [orcid.org/0000-0003-1787-1040](https://orcid.org/0000-0003-1787-1040)

Complete contact information is available at: <https://pubs.acs.org/doi/10.1021/jacs.3c05380>

### Author Contributions

The manuscript was written through contributions of all authors.

### Notes

The authors declare no competing financial interest.

## ■ ACKNOWLEDGMENTS

This work was supported by fundings from the National Science Foundation (DMR-1904701). PSH thanks the Welch Foundation (Grant E-1457) and the National Science Foundation (DMR-2002319) for support. Single-crystal X-ray diffraction data were acquired at IMSERC at Northwestern University, which has received support from the Soft and

Hybrid Nanotechnology Experimental (SHyNE) Resource (NSF ECCS-1542205), the State of Illinois, the International Institute for Nanotechnology (IIN), and the National Science Foundation (DMR-0521267). The authors thank Dr. C. D. Mallikas and Ms. C. Stern for experimental assistance.

## ■ REFERENCES

- Halasyamani, P. S.; Poeppelmeier, K. R. Noncentrosymmetric Oxides. *Chem. Mater.* **1998**, *10*, 2753.
- Kim, E.; Lee, D. W.; Ok, K. M. Centrosymmetric  $[\text{N}(\text{CH}_3)_4]_2\text{TiF}_6$  vs. Noncentrosymmetric Polar  $[\text{C}(\text{NH}_2)_2]_2\text{TiF}_6$ : A Hydrogen-Bonding Effect on the out-of-Center Distortion of  $\text{TiF}_6$  Octahedra. *J. Solid State Chem.* **2012**, *195*, 149.
- Eaton, D. F. Nonlinear Optical Materials. *Science* **1991**, *253*, 281.
- Weis, R. S.; Gaylord, T. K. Lithium Niobate: Summary of Physical Properties and Crystal Structure. *Appl. Phys. A: Mater. Sci. Process.* **1985**, *37*, 191.
- Ding, F.; Nisbet, M. L.; Yu, H.; Zhang, W.; Chai, L.; Halasyamani, P. S.; Poeppelmeier, K. R. Syntheses, Structures, and Properties of Non-Centrosymmetric Quaternary Tellurates  $\text{BiMTeO}_6$  ( $\text{M} = \text{Al, Ga}$ ). *Inorg. Chem.* **2018**, *57*, 7950.
- Welk, M. E.; Norquist, A. J.; Arnold, F. P.; Stern, C. L.; Poeppelmeier, K. R. Out-of-Center Distortions in  $\text{D}^0$  Transition Metal Oxide Fluoride Anions. *Inorg. Chem.* **2002**, *41*, 5119.
- Gautier, R.; Gautier, R.; Chang, K. B.; Poeppelmeier, K. R. On the Origin of the Differences in Structure Directing Properties of Polar Metal Oxyfluoride  $[\text{MO}_x\text{F}_{6-x}]^{2-}$  ( $x = 1, 2$ ) Building Units. *Inorg. Chem.* **2015**, *54*, 1712.
- Donakowski, M. D.; Gautier, R.; Lu, H.; Tran, T. T.; Cantwell, J. R.; Halasyamani, P. S.; Poeppelmeier, K. R. Syntheses of Two Vanadium Oxide–Fluoride Materials That Differ in Phase Matchability. *Inorg. Chem.* **2015**, *54*, 765.
- Pinlac, R. A. F.; Stern, C. L.; Poeppelmeier, K. R. New Layered Oxide–Fluoride Perovskites:  $\text{KNaNbOF}_5$  and  $\text{KNaMO}_2\text{F}_4$  ( $\text{M} = \text{Mo}^{6+}$ ,  $\text{W}^{6+}$ ). *Crystals* **2011**, *1*, 3.
- Ding, F.; Nisbet, M. L.; Zhang, W.; Halasyamani, P. S.; Chai, L.; Poeppelmeier, K. R. Why Some Noncentrosymmetric Borates Do Not Make Good Nonlinear Optical Materials: A Case Study with  $\text{K}_3\text{B}_5\text{O}_8(\text{OH})_2$ . *Inorg. Chem.* **2018**, *57*, 11801.
- Mutailipu, M.; Poeppelmeier, K. R.; Pan, S. Borates: A Rich Source for Optical Materials. *Chem. Rev.* **2021**, *121*, 1130.
- Ding, F.; Griffith, K. J.; Zhang, W.; Cui, S.; Zhang, C.; Wang, Y.; Kamp, K.; Yu, H.; Halasyamani, P. S.; Yang, Z.; Pan, S.; Poeppelmeier, K. R.  $\text{NaRb}_6(\text{B}_4\text{O}_5(\text{OH})_4)_3(\text{BO}_2)$  Featuring Noncentrosymmetry, Chirality, and the Linear Anionic Group  $\text{BO}_2^-$ . *J. Am. Chem. Soc.* **2023**, *145*, 4928.
- Yu, H.; Nisbet, M. L.; Poeppelmeier, K. R. Assisting the Effective Design of Polar Iodates with Early Transition-Metal Oxide Fluoride Anions. *J. Am. Chem. Soc.* **2018**, *140*, 8868.
- Ding, Q.; Liu, X.; Zhao, S.; Wang, Y.; Li, Y.; Li, L.; Liu, S.; Lin, Z.; Hong, M.; Luo, J. Designing a Deep-UV Nonlinear Optical Fluorooxosilicophosphate. *J. Am. Chem. Soc.* **2020**, *142*, 6472.
- Wu, C.; Lin, L.; Jiang, X.; Lin, Z.; Huang, Z.; Humphrey, M. G.; Halasyamani, P. S.; Zhang, C.  $\text{K}_5(\text{W}_3\text{O}_9\text{F}_4)(\text{IO}_3)$ : An Efficient Mid-Infrared Nonlinear Optical Compound with High Laser Damage Threshold. *Chem. Mater.* **2019**, *31*, 10100.
- Xiong, L.; Wu, L.-M.; Chen, L. A General Principle for DUV NLO Materials:  $\pi$ -Conjugated Confinement Enlarges Band Gap\*\*. *Angew. Chem., Int. Ed.* **2021**, *60*, 25063.
- Zhang, Z.-P.; Liu, X.; Liu, X.; Lu, Z.-W.; Sui, X.; Zhen, B.-Y.; Lin, Z.; Chen, L.; Wu, L.-M. Driving Nonlinear Optical Activity with Dipolar 2-Aminopyrimidinium Cations in  $(\text{C}_4\text{H}_6\text{N}_3)^+(\text{H}_2\text{PO}_3)^-$ . *Chem. Mater.* **2022**, *34*, 1976.
- Mighell, A. D.; Himes, V. L.; Rodgers, J. R. Space-Group Frequencies for Organic Compounds. *Acta Cryst. A* **1983**, *39*, 737.
- Brock, C. P.; Dunitz, J. D. Towards a Grammar of Crystal Packing. *Chem. Mater.* **1994**, *6*, 1118.

(20) Guerin, S.; O'Donnell, J.; Haq, E. U.; McKeown, C.; Silien, C.; Rhen, F. M. F.; Soulimane, T.; Tofail, S. A. M.; Thompson, D. Racemic Amino Acid Piezoelectric Transducer. *Phys. Rev. Lett.* **2019**, 122, No. 047701.

(21) Gautier, R.; Norquist, A. J.; Poeppelmeier, K. R. From Racemic Units to Polar Materials. *Cryst. Growth Des.* **2012**, 12, 6267.

(22) Guerin, S.; O'Donnell, J.; Haq, E. U.; McKeown, C.; Silien, C.; Rhen, F. M. F.; Soulimane, T.; Tofail, S. A. M.; Thompson, D. Racemic Amino Acid Piezoelectric Transducer. *Phys. Rev. Lett.* **2019**, 122, No. 047701.

(23) Nisbet, M. L.; Pendleton, I. M.; Nolis, G. M.; Griffith, K. J.; Schrier, J.; Cabana, J.; Norquist, A. J.; Poeppelmeier, K. R. Machine-Learning-Assisted Synthesis of Polar Racemates. *J. Am. Chem. Soc.* **2020**, 142, 7555.

(24) McNaught, A. D.; Wilkinson, A. *Compendium of Chemical Terminology*, 2nd edition; Wiley, 1994.

(25) Fábián, L.; Brock, C. P. A List of Organic Kryptoracemates. *Acta Cryst. B* **2010**, 66, 94.

(26) Clevers, S.; Coquerel, G. Kryptoracemic Compound Hunting and Frequency in the Cambridge Structural Database. *CrystEngComm* **2020**, 22, 7407.

(27) Dalhus, B.; Görbitz, C. H. Non-Centrosymmetric Racemates: Space-Group Frequencies and Conformational Similarities between Crystallographically Independent Molecules. *Acta Cryst. B* **2000**, 56, 715–719.

(28) Moore, J. S.; Lee, S. Crafting Molecular Based Solids. *Chem. Ind.* **1994**, 14, 556.

(29) Breu, J.; Domel, H.; Stoll, A. Racemic Compound Formation versus Conglomerate Formation with  $[M(Bpy)_3](PF_6)_2$  ( $M = Ni, Zn, Ru$ ); Molecular and Crystal Structures. *Eur. J. Inorg. Chem.* **2000**, 2000, 2401.

(30) Potočnák, I.; Burčák, M.; Baran, P.; Jäger, L. Low-Dimensional Compounds Containing Cyano Groups. XI. Preparation, Crystal Structure and Properties of Two Copper(II) Dicyanamide Complexes with  $PF_6^-$  Anions. *Transition Met. Chem.* **2005**, 30, 889.

(31) Zhu, M.; Peng, J.; Pang, H.-J.; Zhang, P.-P.; Chen, Y.; Wang, D.-D.; Liu, M.-G.; Wang, Y.-H. A New 3D Transition-Metal Complex-Templated Framework Based on Wells–Dawson Polyoxometalate and Copper(I)–Pyrazine Moieties. *Inorg. Chim. Acta* **2011**, 370, 260.

(32) Guo, K. K. *Experimental Crystal Structure Determination*. CSD Communication 2020.

(33) Harrison, W. T. A.; Nenoff, T. M.; Gier, T. E.; Stucky, G. D. Tetrahedral-Atom 3-Ring Groupings in 1-Dimensional Inorganic Chains: Beryllium Arsenate Hydroxide Hydrate ( $Be_2AsO_4OH \cdot 4H_2O$ ) and Sodium Zinc Hydroxide Phosphate Hydrate ( $Na_2ZnPO_4OH \cdot 7H_2O$ ). *Inorg. Chem.* **1993**, 32, 2437.

(34) CrysAlisPRO, Oxford Diffraction/Agilent Technologies UK Ltd, Yarnton, England.

(35) Sheldrick, G. M. *SHELXTL, version 6.12.*; Bruker Analytical X-ray Systems, Inc.: Madison, WI, 2000.

(36) Dolomanov, O. V.; Bourhis, L. J.; Gildea, R. J.; Howard, J. A. K.; Puschmann, H. OLEX2: A Complete Structure Solution Refinement and Analysis Program. *J. Appl. Crystallogr.* **2009**, 42, 339.

(37) Spek, A. PLATON, A Multipurpose Crystallographic Tool. *J. Appl. Crystallogr.* **1988**, 21, 983.

(38) Petrović, P. V.; Janjić, G. V.; Zarić, S. D. Stacking Interactions between Square-Planar Metal Complexes with 2,2'-Bipyridine Ligands. Analysis of Crystal Structures and Quantum Chemical Calculations. *Cryst. Growth Des.* **2014**, 14, 3880.

(39) Addison, A. W.; Rao, T. N.; Reedijk, J.; Rijn, J. v.; Verschoor, G. C. Synthesis, Structure, and Spectroscopic Properties of Copper(II) Compounds Containing Nitrogen–Sulphur Donor Ligands; the Crystal and Molecular Structure of Aqua[1,7-Bis(N-Methylbenzimidazol-2'-YL)-2,6-Dithiaheptane]Copper(II) Perchlorate. *J. Chem. Soc., Dalton Trans.* **1984**, 7, 1349.

(40) Nisbet, M. L.; Wang, Y.; Poeppelmeier, K. R. Symmetry-Dependent Intermolecular  $\pi$ – $\pi$  Stacking Directed by Hydrogen Bonding in Racemic Copper-Phenanthroline Compounds. *Cryst. Growth Des.* **2021**, 21, 552.

(41) Melnic, E.; Coropceanu, E. B.; Kulikova, O. V.; Siminel, A. V.; Anderson, D.; Rivera-Jacquez, H. J.; Masunov, A. E.; Fonari, M. S.; Kravtsov, V. C. Robust Packing Patterns and Luminescence Quenching in Mononuclear  $[Cu(II)(Phen)_2]$  Sulfates. *J. Phys. Chem. C* **2014**, 118, 30087.

(42) Wang, Y.; Nisbet, M. L.; Poeppelmeier, K. R. Crystal Structures of Two Copper(1)–6,6'-Dimethyl-2,2'-Bipyridyl (Dmbpy) Compounds,  $[Cu(Dmbpy)_2]_2[MF_6] \cdot xH_2O$  ( $M = Zr, Hf$ ;  $x = 1.134, 0.671$ ). *Acta Cryst. E* **2021**, 77, 819.

(43) Wang, Y.; Fukuda, M.; Nikolaev, S.; Miyake, A.; Griffith, K. J.; Nisbet, M. L.; Hiralal, E.; Gautier, R.; Fisher, B. L.; Tokunaga, M.; Azuma, M.; Poeppelmeier, K. R. Two Distinct Cu(II)–V(IV) Superexchange Interactions with Similar Bond Angles in a Triangular “CuV<sub>2</sub>” Fragment. *Inorg. Chem.* **2022**, 61, 10234.

(44) Wells, A. F. *The Third Dimension in Chemistry*; Clarendon Press, 1956.